Journal of Petroleum Science and Engineering 94–95 (2012) 79–88

Contents lists available at SciVerse ScienceDirect

Journal of Petroleum Science and Engineering

journal homepage: www.elsevier.com/locate/petrol

CFD modeling of the effect of polymer elasticity on residual oil saturation at the pore-scale

Ali Afsharpoor [a], Matthew T. Balhoff [a,*], Roger Bonnecaze [b,1], Chun Huh [a]

[a] Petroleum and Geosystems Engineering, The University of Texas at Austin, 1 University Station C0300 Austin, TX 78712-0228, USA
[b] Department of Chemical Engineering, The University of Texas at Austin, 1 University Station C0400 Austin, TX 78712-0231, USA

ARTICLE INFO

Article history:
Received 28 December 2011
Accepted 14 June 2012
Available online 26 June 2012

Keywords:
Viscoelastic flow
Residual oil saturation
Normal forces
Pore-scale model
CFD modeling

ABSTRACT

Polymers are used in enhanced oil recovery (EOR) to increase sweep efficiency, but recent experimental and field data suggest that viscoelastic polymers such as hydrolyzed polyacrylamide (HPAM) reduce residual oil saturation as well. The observed reduction contradicts decades of belief that polymers could not be used to reduce residual oil because the additional pressure required to overcome capillary pressure is orders of magnitude greater than provided by the more viscous polymer. However, additional forces (such as normal stress forces) may be significant for viscoelastic fluids that are ignored in analysis of purely viscous fluids.

We perform computational fluid dynamics (CFDs) simulations of viscoelastic flow around static oil droplets in geometries representative of pore throats. We show that normal forces are significant for viscoelastic fluids and increase with *De* and the total force imposed on the droplet may be larger than an equivalent Newtonian fluid with the same viscosity. Results indicate that normal forces could dominate and the total, effective force would be enough to mobilize trapped oil.

1. Introduction and background

The flow of viscoelastic fluids in porous media is important in many applications including composite manufacturing in fibrous materials (Skartis et al., 1992; Preziosi et al., 1996), filtration of polymer solutions (Kozicki and Kuang, 1994), removal of liquid pollutants in soils (Londergan et al., 2001; Sochi, 2009), blood flow in capillaries (Thurston, 1974; Canic et al., 2006; Rojas, 2007), and enhanced oil recovery (EOR). In EOR polymer flooding is one process used to improve the sweep efficiency in oil reservoirs. The additional viscosity of the polymer solution allows for a more piston-like displacement of oil and results in additional recovery.

1.1. Effect of viscoelastic polymers on residual oil saturation

Despite the use of polymers to improve sweep efficiency, conventional wisdom has suggested that they could not be used to reduce residual oil saturation (Lake, 1989; Sorbie, 1991; Willhite and Green, 1998). At the pore-scale, capillary forces play an important role and can prevent the non-wetting phase from flowing. Capillary force by a snap-off mechanism makes the oil phase unconnected and difficult to mobilize. It is believed that trapped oil is restricted from being drawn out of the tight pores because the pressure force across the oil droplet in water or polymer flooding is not high enough to overcome the capillary pressure forces. If the pressure gradient were sufficiently high, the oil droplet would stretch out toward the adjacent pore, squeeze through the constriction, and then flow to the next pore.

It is believed that the additional viscosity of polymers would not provide nearly enough pressure drop to overcome capillary forces and mobilize a significant amount of residual oil. This is true for a purely viscous Newtonian fluid and can be demonstrated using simple calculations. For example, consider a typical water-wet reservoir (contact angle, $\theta=0^\circ$), relative permeability (k_w) of 100 mD, and a 1 cp viscosity (μ) fluid flowing at a Darcy velocity (v_w) of 1 ft/day. The applied pressure gradient would be less than 0.1 psi/ft. For a typical pore geometry with length 50 μm, throat radius of 10 μm, pore body radius of 50 μm, and surface tension (σ) of 30 dynes/cm, the required pressure gradient to mobilize the residual oil is approximately 4000 psi/ft; about 4–5 orders of magnitude higher than the applied pressure gradient. Using a more viscous fluid (EOR polymers are usually 10–100 cp) would provide additional pressure gradient, but it would still be at least two orders of magnitude less than required to reduce residual oil saturation (Stegemeier, 1974).

Despite this fundamental understanding of strong capillary forces and decades of belief that polymers should have no impact on residual saturation, both experimental and field observations have suggested that viscoelastic polymers (specifically hydrolyzed

* Corresponding author. Tel.: +512 471 3246; fax: +512 471 9605.
E-mail address: Balhoff@mail.utexas.edu (M.T. Balhoff).
[1] Tel.: +512 471 5238; fax: +512 471 7060.

0920-4105/$ - see front matter © 2012 Elsevier B.V. All rights reserved.
http://dx.doi.org/10.1016/j.petrol.2012.06.027

polyacrylamide (HPAM)) are effective at reducing residual oil and improving recovery by as much as 20% additionally. Wreath (1989) and then Wang (1995) showed decreased residual oil saturation in corefloods using HPAM in strongly water-wet Antolini sandstones when compared to waterfloods or even floods using inelastic polymers (e.g. Xanthan gum). Residual oil was reduced significantly (up to 22%) in the experiments by Wang (1995). Reduced residual oil using viscoelastic polymers in corefloods of water-wet media was also found by Zaitoun and Kohler (1987, 1988), Schneider and Owens (1982), and Bakhitov et al. (1980). Similar observations have been found in mixed-wet and oil-wet experiments (Wang et al., 2010) and field studies (Putz et al., (1988); Wang (2000)).

A few hypotheses have been proposed for the observed reduction of residual oil, including accelerated drainage of oil films on rock surfaces, scoured oil in dead-end pores, and trapped oil pulled out in stable oil threads (Wang et al., 2001; Huh and Pope, 2008). Adding polymer to water causes an increase in both macro and micro scale sweep efficiency. Wang (2000) showed higher molecular weight and higher concentrations of polymer result in higher elasticity. They hypothesized that the higher molecular weight causes a reduction in maximum velocity, so a velocity gradient at the wall increases, resulting in stripping off oil from the pore walls. In dead-end pores, the elasticity of polymer results in dragged oil and may further reduce the residual oil saturation. For water-wet media in particular, the elasticity of the fluid may help prevent snap-off (or re-connects snapped-off fluid). The non-wetting oil phase can then be pulled through the pore throat as a stable thread. The simulations conducted in this work test this hypothesis, in which wetting fluid flows around an oil droplet.

To investigate the displacement efficiency (E_D), the micro forces are neglected for fluids without elastic effects. This is a reasonable assumption because the micro forces are negligible compared to viscous forces which are proportional to pressure gradient (Wang et al., 2010). Micro forces are categorized into two forces, normal force and kinetic force which are both caused by change in flow lines in pore bodies. Experiments and simulation show that flow lines for viscoelastic fluids are significantly different from those of Newtonian fluids. Viscoelastic fluids behave like an elastic solid as well as viscous fluid; the elastic behavior leads to flow lines that appear as an expanding and contracting piston flow. Wang et al. (2000) showed that micro forces for viscoelastic fluid flow are comparable to macro forces, which should be considered in analysis of fluid dynamics. They also showed that only the first normal force differential and its corresponding Weissenberg number (or equivalently Deborah number, *De*) affect the shape of the flow lines; other elastic properties and the viscosity of the driving fluid do not affect flow lines, therefore they do not affect the E_D. They predicted that the capillary number and viscoelasticity both influence the displacement efficiency and residual oil saturation.

1.2. Mathematical modeling of viscoelastic flow in porous media

Modeling viscoelastic flow in the presence of trapped oil at the pore scale could better explain the fundamental reasons for reduction in residual oil. Furthermore, this could lead to new EOR strategies and the design and synthesis of polymers with optimal rheological properties. Several authors have studied single-phase viscoelastic fluids experimentally and numerically in both porous media and constrictions representative of pores. Marshall and Metzner (1967) presented a model for viscoelastic flow in porous media as a function of the dimensionless *De* ($=\lambda/t_r$); where λ is relaxation time and t_r is the residence time. They performed experimental tests in packed beds of spheres and supported the analysis. They observed the deviation from the drag coefficient-Reynolds number relationships for a purely viscous fluid at the critical value of *De* which depends on different variables such as homogeneity. Deiber and Schowalter (1981) used the method of geometric iteration to solve the momentum equation for a Maxwell fluid through sinusoidal ducts. They observed a higher flow resistance than expected from purely viscous fluids at high flow rate, and this effect is the result of fluid elasticity, even without a secondary flow. Later, Gupta and Sridhar (1985) analytically evaluated stress of polymer solutions through a tube having a periodically varying diameter. They found that if the deformation rate is assumed constant, the stress depends not only upon *De*, but also on the aspect ratio.

Other authors numerically studied the extensional effects of viscoelastic fluids in planar and axi-symmetric contraction/expansions (Rajagopalan et al., 1990; Fan et al., 1999; Alves et al., 2003; Binding et al., 2006; Aguayo et al., 2008) and reported shear-thickening behavior. Several attempts have been made to overcome convergence issues for this highly nonlinear problem to reach a higher *De* number. For instance, Huang and Feng (1995) used POLYFLOW software to simulate the viscoelastic fluid flow around a sphere placed in a cylindrical tube. They used an EVSS (elastic–viscous stress split) formulation for stress and unstructured triangle meshing to reach $De\sim 2.5$. In the EVSS interpolation, the constitutive equation is not solved in terms of the viscoelastic extra-stress tensor. Instead, the viscoelastic extra-stress tensor is split into purely viscous and elastic components. This split form is substituted into the constitutive equation, which is re-written in terms of the elastic component and solved. Combining both viscous and elastic components recovers the actual viscoelastic stress tensor. Further details on the EVSS method can be found in Van Schaftingen and Crochet (1984) and Rajagopalan et al. (1990).

Binding et al. (2006) studied the Olydroyd-B model for a 4:1 contraction (channel geometry which abruptly constricts by a factor of four), and 4:1:4 cases (geometry also expands after constriction). Pressure drop was calculated using POLYFLOW software for both planar and axisymmetric contraction–expansion cases. They also used the EVSS (elastic–viscous split stress) formulation for stress calculation. They observed that the pressure drop initially reduces with *De* as the elasticity increases but as *De* number is further increased, it eventually rises significantly above the equivalent Newtonian pressure drop. Several authors have reported this same trend; Webster et al. (2004) conducted the simulations for Olydroyd-B and Phan-Thien Tanner (PTT) models and showed linear declining of pressure drop with increasing *De*. Szabo et al. (1997) studied an Oldroyd-B fluid and finitely extensible nonlinear elastic (FENE) model and observed a similar result.

Here we model the flow of viscoelastic fluids around oil droplets in converging/diverging pore throats with the goal of obtaining a fundamental understanding of the micro forces imposed on the droplet. Additional normal forces, not present for purely viscous fluids, may explain the observed decrease in residual oil saturation in core flood experiments and field studies. Section 2 of this paper describes the mathematical and numerical approach used to solve the nonlinear problem of viscoelastic flow around oil droplets in a converging and diverging throat. Section 3 presents qualitative pictures of the flow fields and stresses as well as quantitative results of the forces present on a droplet for a Newtonian versus a viscoelastic fluid at various *De*. These results are discussed along with possible explanations for reduced residual oil saturation. Finally, Section 4 presents some conclusions drawn from this work as well as proposed future studies.

2. Mathematical and numerical approach

In order to better understand the observed decrease in residual oil in experiments and field data, CFD modeling is performed here for viscoelastic flow around stationary oil droplets. The hypothesis of this work is that large normal forces in viscoelastic fluid flow leads to

formation of stable oil threads which draw the trapped oil out of the tight pore structure. Extra normal forces due to normal stress may become significant for viscoelastic flow and push the trapped oil droplet. Only increasing the viscosity by adding polymer is insufficient to mobilize the trapped oil; therefore, other phenomena at the pore level must contribute to the observed mobilization of the oil. In porous media, the wetting phase (e.g., polymer-containing water) flows along the walls and non-wetting phase (e.g., oil phase) flows at the center of the pore. CFD modeling is used here to simulate two-phase flow in geometries approximating pore throats (sinusoidal ducts) to understand the fundamental physics of viscoelastic fluid dynamics at the pore level. This geometry keeps the model simple, but provides the required characteristics of a pore throat to investigate viscoelastic flow. In order to observe elastic effects, geometry with varying cross-section, perpendicular to the flow direction, is needed.

A viscoelastic fluid is a non-Newtonian fluid which exhibits both viscous liquid and elastic solid characteristics simultaneously. A viscoelastic fluid has a memory and partially returns to initial state after deformation; the dimensionless Deborah number (*De*) is used to describe the ratio of elastic to viscous effects. We define *De* here for converging/diverging ducts as follows:

$$De = \frac{Q\lambda}{\pi R_t^3}, \tag{1}$$

where Q is volumetric flow rate, λ is the polymer molecule's relaxation time, and R_t is the narrowest radius of the pore throat. Elastic effects are negligible for $De \ll 1$; at large *De*, first normal stress differences play an important role, which leads to extensional viscosity effects that dominate over shear viscosity (Macosko, 1994). Extensional flows are those that occur as a result of normal stresses as opposed to shear stresses (which result in shear flows). The extensional viscosity is defined as the first normal stress difference divided by the rate of strain. The ratio (Trouton) of extensional viscosity to shear viscosity is 3 for simple fluids but can be much higher for fluids exhibiting nonlinear viscoelasticity.

In this study the upper convected Maxwell (UCM) model (Eq. (2)) is used as the constitutive equation for the non-Newtonian fluid, which is given by

$$\lambda\left[\frac{\partial\tau}{\partial t} + (u\cdot\nabla)\tau - \nabla u\cdot\tau - \tau\cdot\nabla u^T\right] + \tau = \eta(\nabla u + \nabla u^T) \tag{2}$$

It has been suggested that an UCM reasonably describes the rheology of HPAM and a modified upper-convected Maxwell model (MUCM) was represented by Yin et al. (2006) to include the non-Newtonian shear-thinning behavior. The goal of this work is not necessarily predictive in nature, but rather to obtain a fundamental understanding of the micro forces on an oil droplet. This could be accomplished with any viscoelastic fluid; the UCM is chosen because of its relative simplicity.

The rheological model (2) can be directly substituted into the momentum Eq. (3) and coupled with the continuity Eq. (4). With the exception of very simplified geometries and low *De*, these equations cannot be solved analytically. For more complex geometries (such as the sinusoidal pore throat used here), numerical methods such as the finite element method (FEM) must be implemented.

$$\rho\left[\frac{\partial u}{\partial t} + (u\cdot\nabla)u\right] = -\nabla P + \nabla\cdot\tau \tag{3}$$

$$\nabla\cdot u = 0 \tag{4}$$

Fig. 1 shows schematic figures of throat geometries used in this work. The geometry is 2D axisymmetric and the problems solved were steady state with both fixed inlet/outlet flow rates (both fixed pressure and flow rate boundary conditions have been tested). The

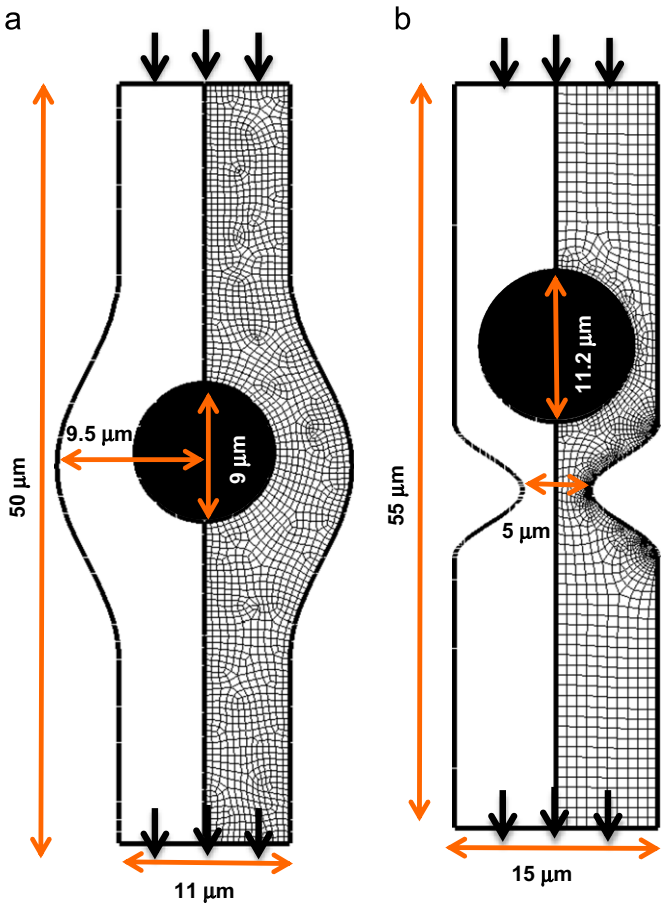

Fig. 1. Schematic of simulation geometries and mesh arrangements for (a) pore-centered geometry and (b) constriction geometry.

fluid flows from top to bottom in Fig. 1 and different forces acting on the stationary oil droplet are evaluated in the results section. The geometry is sinusoidal, but with the in-flow and out-flow zone lengths extended to ensure fully-developed flow. Since the geometry is axisymmetric, only half of the domain is modeled and a symmetry boundary condition is employed at $r=0$.

Solution of the momentum equations for viscoelastic flow is difficult because it is a highly nonlinear problem; in most practical cases ($De > 1$; converging/diverging geometry) the problem exhibits strong singularities. Therefore the problem is numerically difficult to solve in terms of both stability and convergence (Huang and Feng, 1995; Hulsen et al., 2005). In this work, ANSYS POLYFLOW software has been used to solve this complicated numerical problem.

Sensitivity analysis has been performed to determine mesh refinement such that further refinement does not affect the solution. The number of elements and mesh configurations are different for different cases as discussed in the results and discussion section. Among various boundary conditions, fixed pressure and fixed volumetric flow rate have been tested for inlet and outlet. No-slip conditions for the pore wall and stationary oil droplet are applied.

3. Results and discussion

Numerical simulations were performed with the geometries shown in Fig. 1. The fluid was described by the upper-convected Maxwell model (UCM) with rheological properties, $\lambda = 0$ to 0.25 s and $\mu = 40$ cp (0.04 Pa-s). The *De* number can be controlled by

either changing the relaxation time (done here) or inlet/outlet boundary condition values (pressure drop or flow rate) across the throat. Two locations of the oil droplet are studied: (1) in the center of a pore and (2) upstream of a constriction. The first geometry (depicted in Fig. 1a) is referred to as "pore-centered geometry" and is interesting because of the symmetry in the *z*- and *r*- directions. The second geometry (depicted in Fig. 1b) is referred to as "constriction geometry" and may be more realistic as it represents a droplet that requires force to be squeezed through a constriction.

In all simulations the oil droplet was stationary and of fixed size. This idealized case might correspond to a situation where capillary forces are so strong that the forces acting on the droplet (pressure or normal stress) are not significant and therefore are unable to mobilize the droplet or change the shape (even for the viscoelastic fluid). The geometry is hypothetical, but nonetheless provides the insight needed to understand the fundamental physics driving reduced residual oil saturation in the presence of fluids that are elastic.

3.1. Pore-centered geometry

Fig. 1(a) depicts the dimensions of the pore geometry. The first set of simulations involved fixed flow rate boundary conditions of $Q=1\times10^{-14}$ m^3/s (approximate Darcy velocity of 1 ft/day). The mesh arrangement has 1798 nodes and 1647 elements for the simulations of this geometry with a fixed flow rate boundary condition. The mesh configuration is shown in Fig. 1(a).

Fig. 2 shows the pressure fields for both a Newtonian fluid ($De=0$) and viscoelastic fluids ($De=0.4$, 0.7, and 1.4 respectively). The results show that the pressure field for viscoelastic fluids is non-symmetric. This asymmetry increases with *De* and is due to the elastic behavior of the fluid. Unlike a Newtonian fluid which instantaneously relaxes when a stress is imposed, viscoelastic fluids have memory; they require time to return to their original shape. Past the droplet, a distorted pressure field for high *De* occurs. Further downstream, the pressure field is more symmetric because the fluid has sufficient residence time to relax.

For similar reasons, a low-pressure pocket exists ahead of the oil droplet which results in the local pressure gradient across the oil droplet to be more than the average pressure gradient in the pore body along the symmetrical axis. The pocket ahead of the oil droplet is due to secondary flow/eddies formed under elastic conditions. The fluid is unable to instantaneously relax as it passes the oil droplet. The flow streamlines are therefore more tangential to the pressure gradient and the lack of flow ahead of the droplet results in a low pressure. We note that the low-pressure pocket does not necessarily imply that the pressure force is higher for viscoelastic flow than Newtonian flow because the pressure force is the line integral of pressure over droplet surface. For this particular geometry and boundary condition, the pressure force is higher for higher *De* (Table 1), but in subsequent simulations the opposite behavior is observed.

Figs. 3 and 4 show the velocity field and normal stress field, respectively, for the same *De* numbers as depicted in Fig. 2. The velocity field for viscoelastic fluids is non-symmetric and the velocity is higher near the center. The velocity field is distorted downstream of the oil droplet at higher *De*; this asymmetry is expected behavior and is a direct result of the normal forces. The normal stress is negligible for the Newtonian fluid compared to viscoelastic fluid, especially around the oil droplet; this effect is more pronounced as the *De* number increases. Normal stress forces for Newtonian fluids are typically neglected when determining local forces and equilibrium conditions on a droplet (Lake,

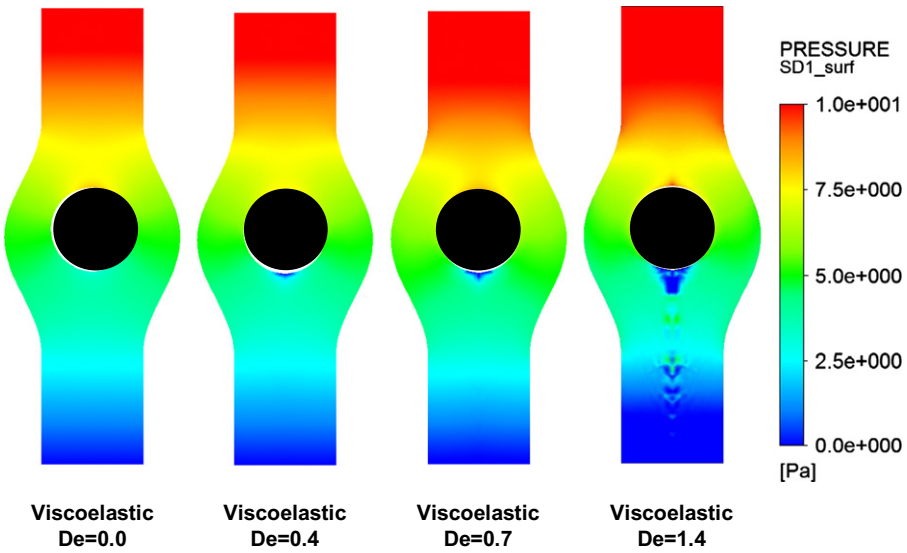

Fig. 2. Pressure field in the pore throat for (a) Newtonian fluid ($De=0$), (b) Viscoelastic fluid ($De=0.4$), (c) Viscoelastic fluid ($De=0.7$) (d) Viscoelastic fluid ($De=1.4$).

Table 1
Summary of micro-forces presented on an oil droplet in the presence of Newtonian and viscoelastic fluids for the pore-centered geometry and fixed flow rate boundary condition.

	VE, $De=1.4$	VE, $De=0.7$	VE, $De=0.4$	Newtonian
Overall pressure drop (Pa)	937	816	766	759
Pressure drop across oil droplet (Pa)	1632	1208	557	342
Pressure force (N)	2.22E-06	1.51E-06	1.34E-06	1.24E-06
Normal stress Force (N)	8.82E-07	2.00E-07	2.44E-08	5.73E-08
Total (N)	3.10E-06	1.71E-06	1.36E-06	1.29E-06

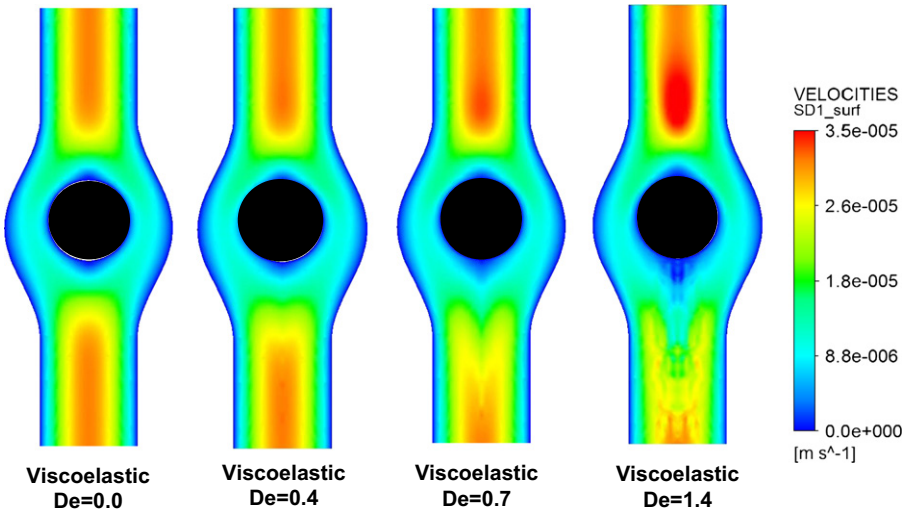

Fig. 3. Velocity field in the pore throat for (a) Newtonian fluid ($De=0$), (b) Viscoelastic fluid ($De=0.4$), (c) Viscoelastic fluid ($De=0.7$), and (d) Viscoelastic fluid ($De=1.4$).

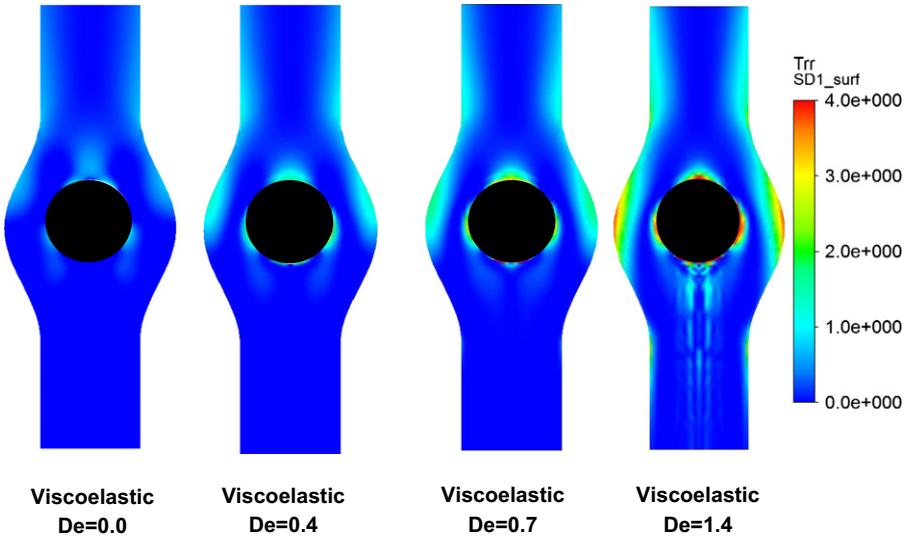

Fig. 4. Normal stress field in the pore throat for (a) Newtonian fluid ($De=0$), (b) Viscoelastic fluid ($De=0.4$), (c) Viscoelastic fluid ($De=0.7$), and (d) Viscoelastic fluid ($De=1.4$).

1989). However, for the viscoelastic fluid, normal forces are significant even at the relatively low *De* studied here. These normal forces are likely much more significant at the higher *De* observed in EOR processes. Unfortunately, the strong nonlinearities of the problem prevent modeling at *De* larger than performed here. Attempts to model viscoelastic fluids at higher *De* (or Weisenberg number) continues to be a challenge in all disciplines, and numerical algorithms to solve this nonlinear problem continue to be developed (Hulsen et al., 2005).

Table 1 compares the forces due to pressure and normal stress for the Newtonian and viscoelastic fluids. The table shows that both pressure and normal stresses increase with *De* for this geometry and therefore the total force imposed on the droplet increases with *De*. At the relatively low *De* investigated here ($De<1.5$), normal stress forces are still an order-of-magnitude smaller than pressure forces. However, the normal forces are increasing at a much faster rate than pressure forces. In the applications of EOR, a common range of shear rates (1–10 $1/s$) in pore throats and range of relaxation times (0.01–15 s) for polymers used in the field, the *De* number can be significant for a typical pore throat size of 1 μm (Heemskerk et al., 1984; Cannella et al., 1988; Masuda et al., 1992; Garrocuh and Gharbi, 2006; Delshad et al., 2008; Lee et al., 2009; Kim et al., 2010). It is likely that at this higher *De*, normal forces would dominate over pressure forces and could result in mobilization of residual oil. In the extreme case of near–wellbore flow, $De=O(100)$ may be observed due to the very high velocities. Although the near-wellbore region represents only a small portion of recoverable oil, extremely high *De* are observed.

3.2. Constriction geometry

A simulation geometry is employed in which the oil droplet is bigger than the pore throat (Fig. 1b). Simulations in this geometry are numerically more challenging than the former (pore-centered geometry) because the fluid contraction at the narrowest radius representing the pore throat leads to high elasticity in that region and makes it numerically difficult to solve. The required mesh is extremely fine. Quadrilateral element shape with 1960 nodes and 1790 elements was found to be an efficient mesh arrangement for this specific geometry.

Fig. 5 shows the pressure field for a Newtonian fluid and viscoelastic fluids at different *De* numbers for a fixed flow rate boundary condition ($Q=1\times10^{-15}$ m^3/s). As the *De* number increases, the overall pressure drop across the entire pore increases, and a low-pressure pocket starts to form in front of the oil droplet. Unlike the pore-centered geometry, the low-pressure pocket does not lead to more pressure force across the droplet for viscoelastic fluids at higher *De*. The summary of force balances are tabulated in Table 2.

It should be noted that the viscosity is the same (40 cp) for all simulations, regardless of whether the fluid is Newtonian or viscoelastic, in order to isolate the effects of normal forces on the oil droplet.

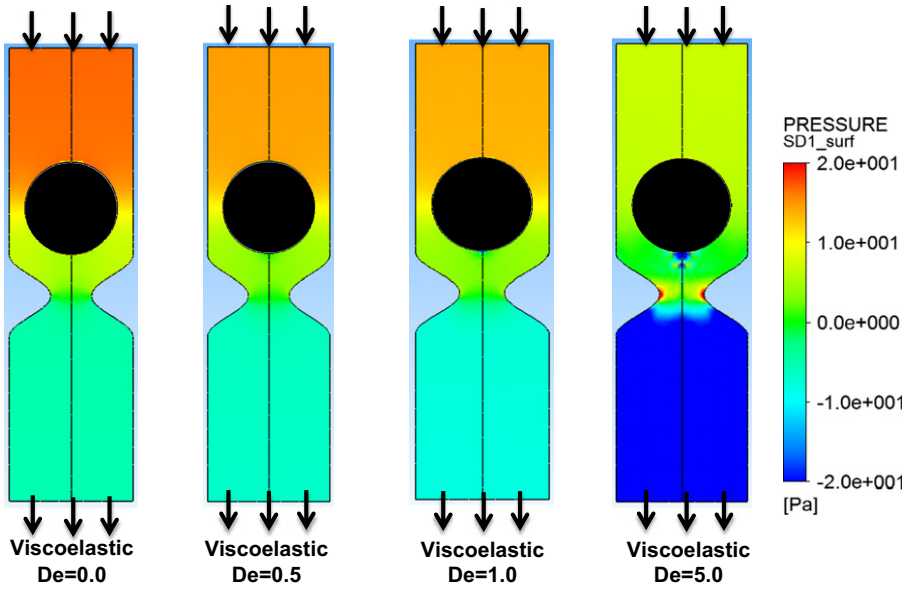

Fig. 5. Pressure field in the pore throat for a (a) Newtonian fluid, (b) Viscoelastic fluid (*De*=0.5), (c) Viscoelastic fluid (*De*=1.0), and (d) Viscoelastic fluid (*De*=5.0).

Table 2
Summary of micro-forces presented on an oil droplet in the presence of Newtonian and viscoelastic fluids for the constricted geometry and constant flow rate boundary conditions.

	VE, *De*=5.0	VE, *De*=1.0	VE, *De*=0.5	Newtonian
Overall pressure drop (Pa)	2105	1098	1065	1108
Pressure drop across oil droplet (Pa)	7579	1655	742	650
Pressure force (N)	3.52E-06	4.65E-06	4.76E-06	4.86E-06
Normal stress force (N)	2.17E-06	4.43E-07	2.32E-07	1.84E-07
Total (N)	5.69E-06	5.09E-06	5.00E-06	5.05E-06

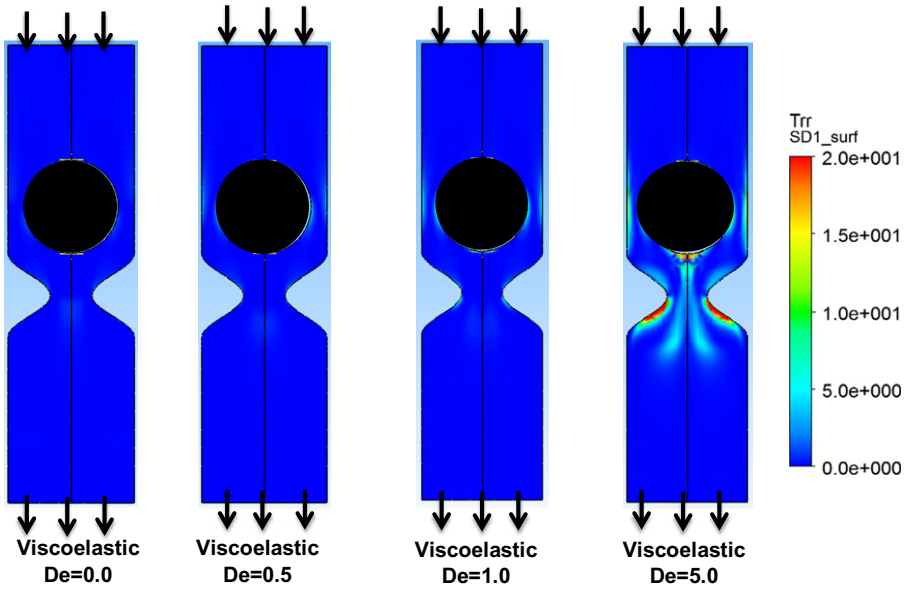

Fig. 6. Normal stresses in the pore throat for a (a) Newtonian fluid, (b) Viscoelastic fluid, (*De*=0.5) (c) Viscoelastic fluid (*De*=1.0) and (d) Viscoelastic fluid (*De*=5.0).

In practice, viscoelastic polymers are also much more viscous (by 1–2 orders of magnitude). Mobilization of oil by viscoelastic polymers may be a result of a combination effects, including additional pressure drop due to an increase in viscosity as well as normal forces that are not significant for purely viscous fluids.

Fig. 6 shows the normal stress field (τ_{rr}) for the same *De* utilized in Fig. 5. As expected the normal stresses are more pronounced as the *De* number increases; accordingly, the normal forces are increasing as summarized in Table 2. Fig. 7 compares the velocity profile for Newtonian and viscoelastic flow at different *De*; it shows that as the fluid becomes more elastic the velocities in the pore throat will be smallest at the center. Fundamentally, due to no-slip boundary condition, for Newtonian fluids, the velocity is higher at the center rather than near the wall; toward the center the velocity increases for the Newtonian fluid. The no-slip condition is still imposed at the wall for viscoelastic flow, but the velocity is increasing near the throat center, further demonstrating the non-symmetric behavior of viscoelastic fluids.

The final simulations were conducted in the constriction geometry for a fixed pressure boundary condition (instead of fixed flow rate). Polymer injection can occur at constant rate or constant pressure conditions. At the pore-level the appropriate boundary conditions may be better represented by a constant rate or constant pressure gradient (regardless of the well constraint). Therefore, for completeness we also investigate constant pressure gradient across pore throats. The pressure drop across the throat utilized here is 10 Pa (corresponds to ~8 psi/ft) in all constant pressure simulations. Increasing the elasticity of the fluid (by increasing the relaxation time) results in an increase in resistance to flow. The mesh arrangement and numerical strategies are the same as the constant-flow simulations in Figs. 5–7. Fig. 8 shows the pressure fields, which appear similar for all *De* across the

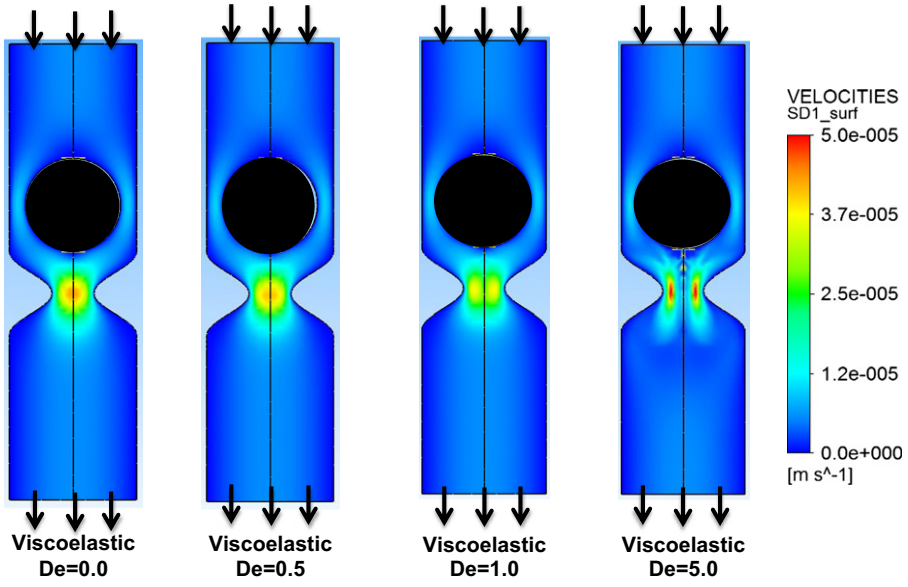

Fig. 7. Velocity field in the pore throat for a (a) Newtonian fluid, (b) Viscoelastic fluid (*De*=0.5), (c) Viscoelastic fluid (*De*=1.0) and (d) Viscoelastic fluid (*De*=5.0).

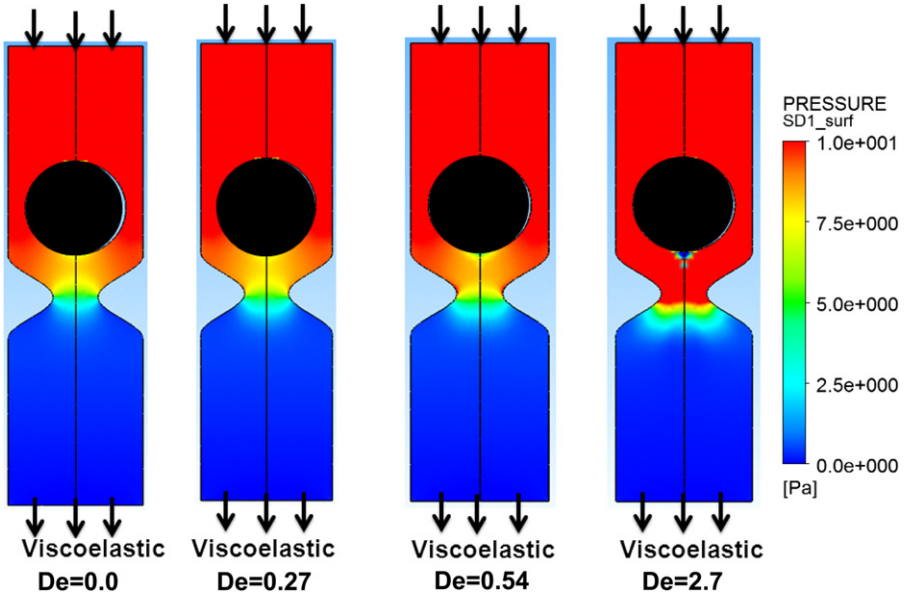

Fig. 8. Pressure field in the pore throat for a constant pressure boundary condition in the constriction geometry for a (a) Newtonian fluid, (b) Viscoelastic fluid, De=0.27, (c) Viscoelastic fluid, De=0.54, and (d) Viscoelastic fluid, De=2.68.

geometry, but the pressures across the oil droplet are different as listed in Table 3.

Fig. 9 shows the normal stress (τ_{rr}) for the different *De* numbers, and as expected the higher the *De* number, the higher the normal stress, even though the flow rate is lower for higher *De* number cases. Fig. 10 compares the velocity profile for Newtonian and viscoelastic flow at different *De* number, which shows as the elasticity increases, the velocity profile at pore throat will be less at the center.

Table 3
Summary of micro-forces presented on an oil droplet in the presence of Newtonian and viscoelastic fluids for a constant pressure boundary condition in the constriction geometry.

	VE, *De*=2.7	VE, *De*=0.53	VE, *De*=0.27	Newtonian
Inlet flow rate (m^3/s)	2.6E-12	4.1E-12	4.1E-12	4.0E-12
Pressure drop across oil droplet (Pa)	3197	1047	1047	529
Pressure force (N)	2.68E-06	4.03E-06	4.03E-06	4.02E-06
Normal stress force (N)	9.51E-07	3.00E-07	2.92E-07	1.50E-07
Total (N)	3.63E-06	4.33E-06	4.32E-06	4.17E-06

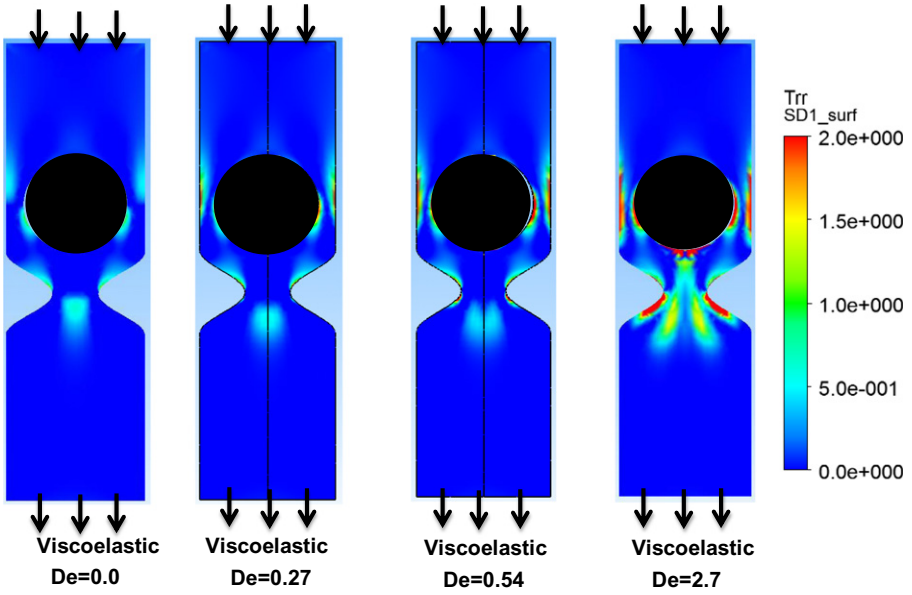

Fig. 9. Normal stresses in the pore throat for a constant pressure boundary condition in the constriction geometry for a (a) Newtonian fluid, (b) Viscoelastic fluid (*De*=0.27) (c) Viscoelastic fluid (*De*=0.54) and (d) Viscoelastic fluid (*De*=2.68).

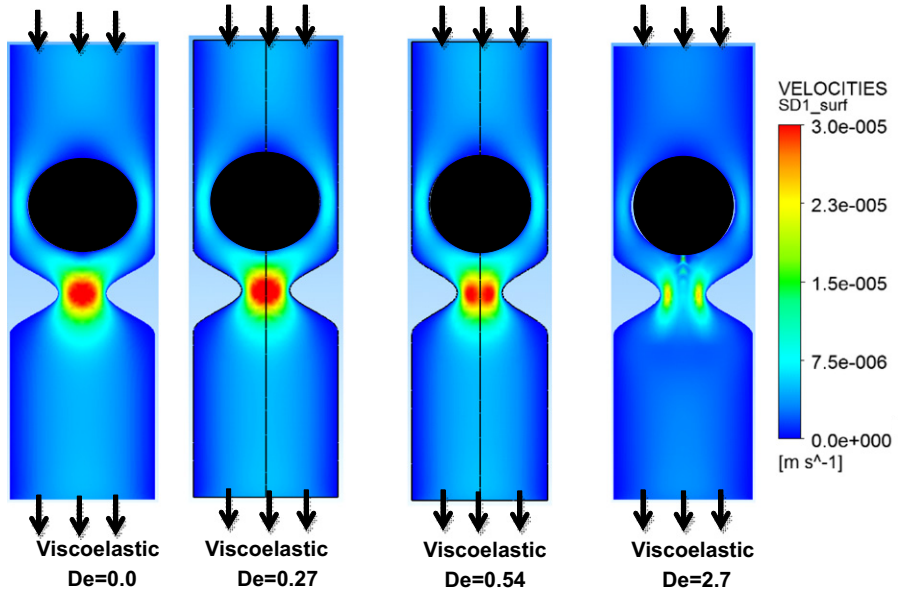

Fig. 10. Velocity field in the pore throat for a constant pressure boundary condition in the constriction geometry for a (a) Newtonian fluid, (b) Viscoelastic fluid (*De*=0.27) (c) Viscoelastic fluid (*De*=0.54) and (d) Viscoelastic fluid (*De* =2.68).

Fig. 11 compares the pressure force and normal stress force as *De* increases for fixed flow rate boundary condition and constriction geometry. As *De* increases, the normal stress force increases, but the pressure force at $De = \sim 3$ starts to decline. However, the total force (which is the summation of pressure force and normal stress force) increases with *De*. The normal stresses increase by a factor of more than 200 and the total normal force increases by a factor of more than 20 between $De = 0$ and $De = 5.0$. Although it cannot be determined definitively, it is very possible that normal forces continue to increase at high *De*, dominate over pressure forces, and the total force continues to increase. These larger normal (and therefore total) forces may be enough to overcome capillary forces and mobilize residual oil in porous media. More likely, it is one of many synergistic factors mobilizing residual oil. For example, the additional viscosity of the polymer would add additional pressure drop and the asymmetry of the flow lines could lead to ganglion pulled off of the droplet.

Fig. 12 shows the pressure force and normal stress force for the fixed pressure boundary condition in the constriction geometry.

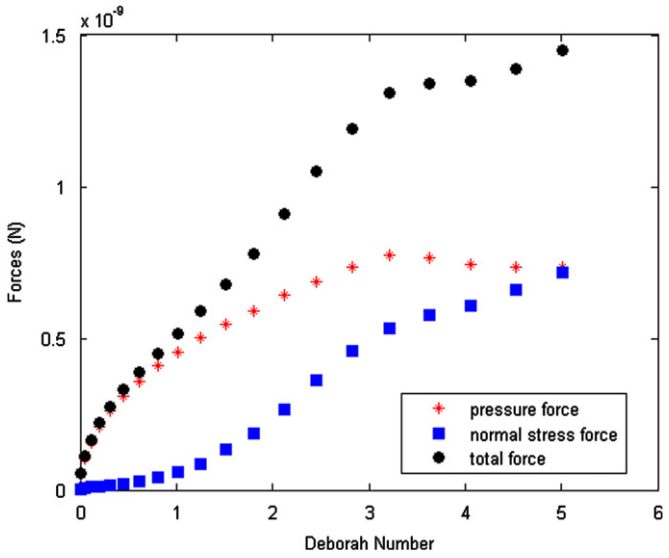

Fig. 11. pressure force, normal stress force and total normal force vs. *De* number for constriction geometry and fixed flow rate inlet/outlet boundary condition.

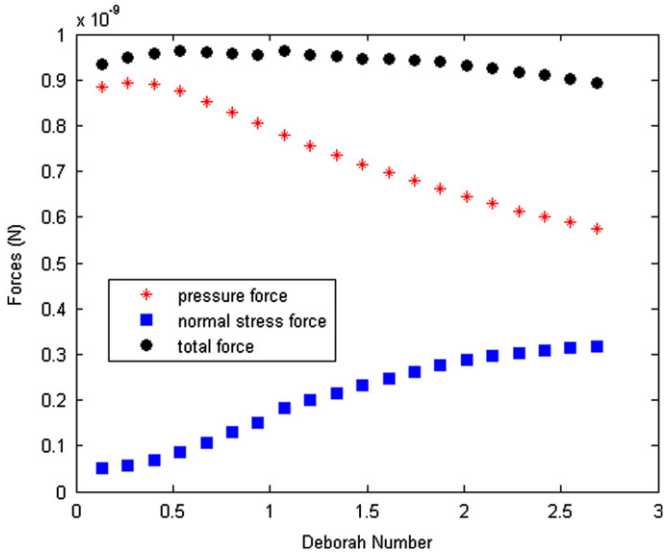

Fig. 12. pressure force, normal stress force and total normal force vs. *De* number for constriction geometry and fixed pressure inlet/outlet boundary condition.

As shown, the normal stress force increases monotonically as *De* increases, but the pressure forces decrease. In Fig. 12 the total normal force is declining in the range of *De* studied, but if the normal force were to increase monotonically, it would eventually dominate the overall pressure force, and total force would also increase. It should also be noted that as the droplet approaches the constriction it would in reality deform. The asymmetric forces on the deformable droplet may be large enough to pull the front end of the droplet into the constriction or tear off ganglion from the droplet. More advanced modeling would be required to study flow around a deformable droplet and test these hypotheses.

It should also be noted that the constant pressure boundary condition is less realistic than the constant rate boundary condition, since polymers are typically injected into wells at constant rates.

4. Conclusions

Pressure gradient alone is not sufficient to overcome capillary forces and mobilize residual oil in reservoirs, even with the increased viscosity of polymers. The recent experimental and field observations that show reduced residual oil in the presence of polymers such as HPAM must be due to other factors, or more likely, combination of forces acting on the oil droplet. Our CFD simulations of viscoelastic flow around static oil droplets in pore throats show that normal stress forces are insignificant for Newtonian fluids, but increase dramatically with *De*. In some cases the total forces imposed on the oil droplet is much larger as a result of these normal forces, even at the moderate *De* studied here. It is possible that at higher *De*, normal forces dominate and the effective force is much larger than a Newtonian fluid with the same viscosity and flowrate. We believe that the observed reduced residual oil is a result of a combination of factors including pressure drop from the high polymer viscosity, normal stress forces in the viscoelastic fluid, and perhaps ganglion pulled off of the droplet due to asymmetry in the flow lines. Future work will focus on modeling these effects in geometries that allow for shape evolution of the droplet as well as complimentary experiments in microfluidics tubes representative of pore throats.

Acknowledgements

The authors would like to thank the financial support of the many companies who participate in the Chemical EOR Industrial Affiliates Project in the Center of Petroleum and Geosystems Engineering (CPGE) (http://www.cpge.utexas.edu/ceor) at the University of Texas at Austin.

References

Aguayo, J.P., Tamaddon-Jahromi, H.R., Webster, M.F., 2008. Excess pressure-drop estimation in contraction and expansion flows for constant shear-viscosity, extension strain-hardening fluids. J. Non-Newtonian Fluid Mech. 153, 157–176.

Alves, M.A., Oliveira, P.J., Pinho, F.T., 2003. Benchmark solution for a olydroyd-B and PTT fluids in planar contractions. J. Non-Newtonian Fluid Mech. 110, 45–75.

Bakhitov, G., Polishchuk, A., Ogandzhayants, V., 1980. Experimental investigation into the influence of polymer additives in water on the relative permeabilities of porous media. Fluid Dyn., 611–615.

Binding, T.M., Phillips, P.M., Phillips, T.N., 2006. Contraction/expansion flows: the pressure drop and related issue. J. Non-Newton. Fluid Mech. 137, 31–38.

Cannella, W.J., Huh, C., Seright, R.S., 1988. Prediction of Xanthan Rheology in Porous Media. SPE 18089. Presented at the SPE Annual Technical Conference and Exhibition, 2–5 October 1988, Houston, Texas.

Canic, et al., 2006. Blood flow in compliant arteries: an effective viscoelastic reduced model, numeric, and experimental validation. Ann. Biomed. Eng. 34 (4), 575–592.

Deiber, J.A., Schowalter, W.R., 1981. Modeling the flow of viscoelastic fluids through porous media. Aiche J. 27, 912–920.
Delshad, M., Kim, D.H., Magbagbeola, O.A., Huh, C., Pope, G.A., Tarahhom, F., 2008. Mechanistic interpretation and utilization of viscoelastic behavior of polymer solutions for improved polymer-flood efficiency. SPE, 113620, In: Presented at the SPE Improved Oil Recovery Symposium, 19–23 April 2008, Tulsa, Oklahoma, USA.
Fan, Y., Tanner, R.I., Phan-Thien, N., 1999. Galerkin/least-square finite-element methods for steady viscoelastic flows. J. Non-Newtonian Fluid Mech. 84, 233–256.
Garrocuh, A.A., Gharbi, R.B., 2006. A novel model for viscoelastic fluid flow in porous media. SPE 102015. In: Presented at the SPE Annual Technical Conference and Exhibition, 24–27 September 2006, San Antonio, Texas, USA.
Gupta, R.K., Sridhar, T., 1985. Viscoelastic effects in non-newtonian flows through porous media. Rheol. Acta 24, 148–151.
Heemskerk, J., Janssen-van Rosmalen, R., Holtslag, R.J., Teeuw, D., 1984. Quantification of viscoelastic effects of polyacrylamide solutions. SPE 12652. In: Presented at the SPE Enhanced Oil Recovery Symposium, 15–18 April 1984, Tulsa, Oklahoma.
Huang, P.Y., Feng, J., 1995. Wall effect on viscoelastic fluids around the circular cylinder. J. Non-Newtonian Fluid Mech. 60, 179–198.
Huh, C., Pope, G.A., 2008. Residual oil saturation from polymer floods: laboratory measurements and theoretical interpretation. SPE 113417, In: Presented at the SPE Improved Oil Recovery Symposium, 19–23 April 2008, Tulsa, Oklahoma, USA.
Hulsen, M.A., Fattal, R., Kupferman, R., 2005. Flow of viscoelastic fluids pasta cylinder at high weissenberg number: stablized simulations using matrix logarithms. J. Non-Newtonian Fluid Mech. 127, 27–39.
Kim, D.H., Lee, S., Ahn, C.H., Huh, C., Pope, G., 2010. Development of a viscoelastic property database for EOR polymers. SPE 129971. In: Presented at the SPE Improved Oil Recovery Symposium, 24–28 April 2010, Tulsa, Oklahoma, USA.
Kozicki, W., Kuang, P.Q., 1994. Cake filtration of suspensions in viscoelastic fluids. Can. J. Chem. Eng. 72 (5), 828–839.
Lake, L., 1989. Enhanced Oil Recovery. Prentice Hall, New Jersey, pp. 2–16, 43–92, 317–353.
Lee, S., Kim, D.H., Huh, C., Pope, G., 2009. Development of Comprehensive rheological property database for EOR polymers. SPE 124798. In: Presented at the SPE Annual Technical Conference and Exhibition, 4–7 October 2009, New Orleans, Louisiana.
Londergan, J.T., Meinardus, H.W., Manner, P.E., Jackson, R.E., Brown, C.L., Dwarakanath, V., Pope, G.A., Ginn, J.S., Taffinder, S., 2001. DNAPL removal from a heterogeneous alluvial aquifer by surfactant- enhanced aquifer remediation. Ground Water Monitoring and Remediation 21 (3), 71–81.
Macosko, C., 1994. Rheology: Principles, Measurements, and Applications. VCH Publishers, Minneapoils.
Marshall, R.J., Metzner, A.B., 1967. Flow of viscoelastic fluids through porous media. Ind. Eng. Chem. Fundam. 6 (3), 393–400.
Masuda, Y., Tang, K., Miyazawa, M., Tanaka, S., 1992. 1D simulation of polymer flooding including the viscoelastic effect of polymer solution. SPE Reservoir Eng., 247–252.
Preziosi, L., Joseph, D., Beavers, G., 1996. Infiltration of initially dry deformable porous media. Int. J. Multiphase Flow 22 (6), 1205–1222.
Putz, A.G., Lecourtier, J.M., Bruckert, L., 1988. Interpretation of high recovery obtained in a new polymer flood in the chateaurenard field. SPE 18093, In: SPE 63rd Annual Technical Conference and Exhibition, Houston, Texas, USA.
Rajagopalan, D., Armstrong, R.C., Brown, R.A., 1990. Finite element methods for calculation of steady, viscoelastic flow using constitutive equations with a newtonian viscosity. J. Non-Newtonian Fluid Mech. 36, 159–192.
Rojas, H., 2007. Numerical implementation of viscoelastic blood flow in a simplified arterial geometr. Medical Eng. Phys. 29, 491–496.
Schneider, F.N., Owens, W.W., 1982. Steady State measurements of relative permeability for polymer/oil systems. SPE J., 79–86.
Skartis, L., Kohomani, B., Kardos, J., 1992. Polymeric flow through fibrous media. J. Rheol. 36 (4), 589–619.
Sochi, T., 2009. Pore-scale modeling of viscoelastic flow in porous media using a Bautista–Manero fluid. Int. J. Heat Fluid Flow 30, 1202–1217.
Sorbie, K.S., 1991. Polymer-Improved Oil Recovery. Blackie, Glasgow and London, pp. 1–5, 37–79.
Stegemeier, G.L., 1974. Relationship of trapped oil saturation to petrophysical properties of porous media. SPE 4754. In: Presented at the SPE Improved Oil Recovery Symposium, 22–24 April 1974, Tulsa, Oklahoma.
Szabo, P., Rallison, J.M., Hinch, E.J., 1997. Start-up of a FENE-fluid through a 4:1:4 constriction in a tube. J. Non-Newtonian Fluid Mech. 72, 73–86.
Thurston, G., 1974. Elastic effects in pulsatile blood flow. Microvasc. Res. 9, 145–157.
Van Schaftingen, J.J., Crochet, M.J., 1984. Int. J. Numerical Meth. Fluids. 4, 1065–1081.
Wang, D., 2000. Viscous-elastic polymer can increase micro scale displacement efficiency in cores. SPE 63227. In: Presented at the 2000 SPE Annual Technical Conference and Exhibition, Dallas, Texas, USA.
Wang, D., Cheng, J., Xia, H., Li, Q., Shi, J., 2001. SPE 72123. Viscous-elastic fluids can mobilize oil remaining after water-flood by force parallel to the oil-water interface. In: Presented at the 2001 SPE Asia Pacific Improved Oil Recovery Conference, Kuala Lumpur, Malaysia.
Wang, D., Xia, H., Yang, S., Wang, G., 2010. SPE 109016. The influence of viscoelasticity on micro forces and displacement efficiency in pores, Cores and in the Field. In: Presented at the 2010 West Asia SPE EOR Conference, Muscat, Oman.
Wang, M., 1995. Laboratory investigation of factors affecting residual oil saturation by polymerflooding. Ph.D. Thesis, University of Texas at Austin.
Webster, M.F., Tamaddon-Jahromi, H.R., Aboubacar, M., 2004. Transient viscoelastic flows in planar contractions. J. Non-Newton. Fluid Mech 118, 83–101.
Willhite, G.P., Green, D.W., 1998. Enhanced Oil Recovery. first edition, SPE text book series, Richardson, Texas.
Wreath, D.G., 1989. A study of polymer flooding and residual oil saturation. M.S. Thesis, University of Texas at Austin.
Yin, H., Wang, D., Zhong, H. 2006. Study on flow behavoirs of viscoelastic polymer solution in micropore with dead end. SPE 101950. In: Presented at the SPE Annual Technical Conference and Exhibition, San Antonio, Texas, USA.
Zaitoun, A., Kohler, N., 1987. The role of adsorption in polymer propagation through reservoir rock. SPE 16274. In: Presented at the SPE Intern. Symp. Oilfield Chem. February 4–6 1987, San Antonio, TX.
Zaitoun, A., Kohler, N., 1988. Two phase flow through porous media: effect of adsorbed polymer layer. SPE 18085. In: Presented at the SPE Annual Technical Conference and Exhibition, 2-5 October 1988, Houston, Texas.